Radiation Physics and Chemistry 155 (2019) 287–290

Contents lists available at ScienceDirect

Radiation Physics and Chemistry

journal homepage: www.elsevier.com/locate/radphyschem

Low temperature synthesis of pure and Fe-doped $HfSiO_4$: Determination of Si and Fe fractions by neutron activation analysis

T.N.S. Sales*, B. Bosch-Santos, M. Saiki, A. Burimova, L.F.D. Pereira, R.N. Saxena, A.W. Carbonari

Nuclear and Energy Research Institute (IPEN-CNEN/SP) University of São Paulo, São Paulo, SP, Brazil

ARTICLE INFO

Keywords:
Hafnia nanoparticles
Hafnon
Fe doping
Neutron activation analysis
Sol-gel

ABSTRACT

A new method of synthesis of hafnium silicate $HfSiO_4$ (also known as hafnon) is reported. We observed a self-controlled incorporation of SiO_2 from the quartz tube in which a sample of hafnium oxide nanoparticles was heated. This approach was then adapted to Fe-doped hafnon production. Sample structure, morphology and composition were characterized by X-ray diffraction, electron microscopy and neutron activation analysis. Diffraction data has shown that lattice parameters of doped $HfSiO_4$ thus obtained are very close to those previously known for bare hafnon. The hafnon-like phase stabilized at T = 900 °C which is about 500 °C lower than the corresponding transition of bare bulk hafnium silicate. The fractions of Si and Fe in the composite matrices were determined with neutron activation analysis. These results completed by X-ray diffraction data allowed to assume that (i) Fe initially substituted Hf in the HfO_2 lattice; (ii) there was no migration of iron atoms from Hf to Si sites at the formation of hafnon-like phase; (iii) doped and undoped hafnium oxide has taken as much Si from the quartz as was needed for the arrangement of $Fe_{1-x}Hf_xSiO_4$ tetragonal system, $0 \leq x < 0.2$. Our results are consistent with those obtained for similar materials, such as metal (Fe,V) doped zircon, where the dopant also demonstrated catalytic effect on phase stabilization.

1. Introduction

The idea to substitute high-κ metal oxides with ceramic gate dielectrics resulted in growing attention to Hf/Zr-based composites (Choi et al., 2011). Due to their advanced properties, among which are thermal and chemical stability, hafnium and zirconium silicates demonstrated potential as environmental barrier coatings and radioactive waste storage matrices (Nakano et al., 2009; Burakov and Anderson et al., 2001). For the field of organic thin film transistors optimization of gate dielectric layer parameters is essential (Klauk, 2010; Veres et al., 2003; Stassen et al., 2004), and an elegant solution was proposed in Chen et al. (2004), where polymer films with embedded metal-oxide nanoparticles (NPs) were introduced. Furthermore, (Hf, Zr, Ti)-oxide NPs were adopted both as alternative to Pt in catalyst layers of polyelectrolyte membrane and microbial fuel cells (Ishihara et al., 2010; Chen et al., 2011; Mecheri et al., 2016) and as dopants for membrane conductivity tuning (Vittadello et al., 2008). We believe that hafnon and zircon powders can bring new degrees of freedom to the development of energy conversion and organic semiconductor technological devices. Therefore, an effective synthesis procedure is the matter of utmost importance.

The formation of $HfSiO_4$ ($ZrSiO_4$) in tetragonal phase implies blending precursor oxides HfO_2 (ZrO_2) and SiO_2 in equimolecular proportions (Curtis et al., 1954; Salt and Hornung, 1967). The temperatures of tetragonal phase formation are reported to be in the 1400–1500 °C range. In this work, however, we present a different strategy to synthesize hafnon-like structures at significantly lower temperature (T~900 °C). We also show that the formation of $HfSiO_4$ can be catalysed by iron ions dissolved in hafnia lattice. Annealing Fe-doped hafnium oxide NPs in a quartz tube caused incorporation of Si sufficient to produce tetragonal phase at $T \leq 900$ °C, as estimated basing on the evolution of diffraction patterns with temperature.

Understanding the roles of Si and Fe in the reaction of HfO_2 powder with the quartz requires a multielement study of composite particles, as well as high-accuracy detection of element concentrations. Although the substitution of host lattice ions by dopants in similar systems was widely discussed in the literature, it remains an open question so far; see, e.g., (Valentin et al., 1999) and references therein. Information on sample structure complemented by elements concentration data can help in verifying whether the ions of iron migrate from Hf to Si sites during the annealing. Because of the nature of the synthesis method adopted in this work, the determination of Si content in the samples with precision is very important. Considering above challenges we employed neutron activation analysis (NAA) – a powerful technique

* Corresponding author.
E-mail address: tatianenas@yahoo.com.br (T.N.S. Sales).

https://doi.org/10.1016/j.radphyschem.2018.06.040
Received 1 August 2017; Received in revised form 18 June 2018; Accepted 21 June 2018
Available online 23 June 2018
0969-806X/

sensitive to trace elements (Amiel, 1981). Gamma-spectroscopy enabled precise determination of silicon and iron concentrations in the composite powder.

2. Experimental

2.1. Sample preparation

The preparation of HfO_2 NPs was carried out using sol-gel method preferred over others due to its low cost and easy particle size control. Hf (99.99% purity) dissolved in diluted hydrofluoric acid, citric acid (CA) of 99.5% and ethylene glycol (EG) of ≥99% purity both from Casa Americana de Artigos para Laboratórios Ltda. were taken in stoichiometric proportion to produce initial colloid. The sol was heated to ~ 100 °C until gel aggregation. Gel was then calcined in air at 550 °C for 14 h in order to eliminate organic material. In what follows we refer to thus obtained NPs as sample (S1).

Fe-doped hafnia powder (S2) was synthesized in a similar manner, except that the initial solution contained $FeCl_2$ (99.99% purity) in addition to hafnium, CA and EG solutions.

2.2. Characterization techniques

2.2.1. X-ray diffraction

X-ray diffraction (XRD) analysis was employed to examine the phase contents of synthesized and annealed samples. Measurements were taken at Bruker D8 Advance 3 kW diffractometer at Multiuser X-ray Diffraction Laboratory (CCN of IPEN-CNEN, Brazil) and at X'pert 2.2 kW diffractometer from Phillips at the Laboratory of Technological Characterization – LCT (Polytechnic college of USP, Brazil) with CuK_α radiation (λ = 1.5418 Å) in Bragg-Brentano configuration at room temperature. Thus obtained XRD patterns were refined with Rietica software.

2.2.2. Electron microscopy

The morphology, texture and speck size of obtained powders were studied with transmission and scanning electron microscopy techniques (TEM and SEM respectively). TEM images were acquired with JEM 2100 instrument by Jeol at the Laboratory of Microscopy and Microanalysis (CCTM of IPEN-CNEN, Brazil). To prepare the samples for TEM analysis the powder was dispersed in 99.5% toluene by Synth and deposited onto 400 mesh carbon coated copper grids. SEM experiments were performed at environmental scanning electron microscope Quanta 650 FEG by FEI of LCT operating at 5 kV accelerating voltage. TEM and SEM images were analyzed using MATLAB software package.

2.2.3. Neutron activation analysis

Two NAA procedures were applied in this study. The concentration of Si was determined by epithermal neutron activation analysis and using short irradiation time. Fe concentration was determined by thermal neutron activation and long irradiation time. The irradiations were carried out at the IEA-R1 pool type nuclear research reactor (IPEN-CNEN, Brazil). The samples and element standards were irradiated in high purity polyethylene capsules with screw caps obtained from Vrije Universiteit (Amsterdam, The Netherlands). The gamma spectrometry was performed using a hyperpure Ge detector, Model GC3020, coupled to a Digital Spectrum Processor DSA 1000, both from Canberra. The energy resolution (FWHM) of the system was 0.90 keV for 122 keV γ-ray peak of ^{57}Co and 1.87 keV for 1332 keV γ-ray peak of ^{60}Co. For counting, the sample and standard were measured in the same geometry. Gamma spectra were collected and processed using Canberra Genie 2000 Version 3.1 software. Elemental concentrations were calculated by comparative method (de Soete et al., 1972).

For Si determination ~ 20 mg of sample and a Si standard (22 mg metallic silicon of 99.999% purity from Alfa Aesar) weighted in polyethylene capsules were placed in a cadmium capsule for irradiation using pneumatic transfer system. The irradiation lasted for 30 s. Thermal, epithermal and fast neutron fluxes at irradiation position were (in $n \cdot cm^{-2} \cdot s^{-1}$) 1.9×10^{12}, 5.4×10^{10} and 3.7×10^{11} respectively. The decay time of about 3 min was required to mount the irradiated samples and standards in tubes for counting for 300 s. The γ-ray energy of 1273.36 keV of ^{29}Al with half-life of 6.56 min formed in the reaction $^{29}Si(n,p)^{29}Al$ was used for Si identification and quantification.

In the case of Fe determination, about 20 mg of the sample and synthetic standard with 3.0015 mg of Fe were irradiated for 8 h under a thermal neutron flux of 4.7×10^{12} $n \cdot cm^{-2} \cdot s^{-1}$. This synthetic standard of Fe was prepared using certified stock standard provided from Spex CertiPrep (USA). The solution was pipetted into a capsule and dried inside a desiccator. The sample and Fe standard were measured after 5d of decay time. The 1099.25 keV peak of ^{59}Fe with a half-life of 44.5d was used to identify ^{59}Fe formed in the reaction $^{58}Fe(n, \gamma)^{59}Fe$.

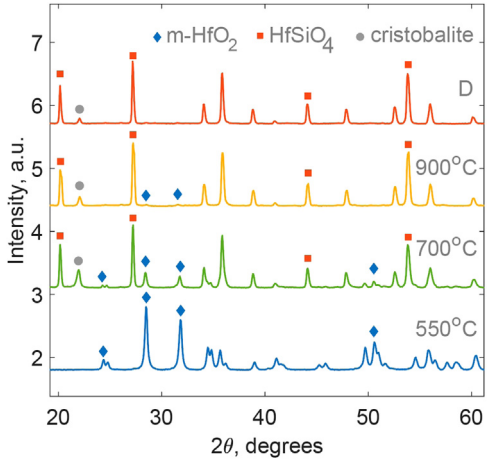

Fig. 1. XRD patterns of HfO_2 after 550 °C calcination (S1), 14 h annealing at 700 °C and 900 °C. Plot D represents the diffractogram of the sample remaining in direct contact with quartz while annealed at 900 °C.

3. Results and discussion

Fig. 1 shows the diffractogram of as prepared (S1) sample together with XRD patterns of (S1) powder annealed at 700 °C and 900 °C in a quartz tube for 14 h. Pattern labeled with D relates to the powder that was in direct contact with the inner surface of the tube during the annealing at 900 °C. The diffractograms clearly reflect structural evolution, the nucleation of hafnon phase in the samples annealed in quartz is accompanied by a strong suppression of the monoclinic phase of hafnia (m-HfO_2). The peak near 2θ = 22° was attributed to cristobalite – tetragonal phase of SiO_2 – t-SiO_2 (Pluth et al., 1985).

To check the structural behavior of SiO_2 of the tubes used for the annealing of hafnia we have macerated a piece of such tube in an agate mortar. XRD data was collected for as prepared quartz crumb and that annealed at 900 °C for 14 h. Silica didn't reveal any trace of ordering due to annealing, and both XRD patterns demonstrated the behavior typical for amorphous composites.

XRD pattern of as prepared (S2) is given in Fig. 2 (lower plot). Similarly to bare hafnia, iron doped sample was annealed in a quartz tube at 900 °C for 14 h, diffractogram of resulting blend also shown in Fig. 2. Theoretical models used for refinement included a single monoclinic phase of HfO_2 for (S2) and tetragonal $HfSiO_4$ phase for annealed sample, which turned out satisfactory for a good fit. Lattice parameters of hafnon-like compound based on Fe doped hafnia were estimated with Rietveld method and match those of undoped hafnon, $a = b = 6.5699(1)$ Å and $c = 5.9649(1)$ Å. XRD did not reveal other contributions except for a barely distinguishable cristobalite peak, which allows to assume that Fe ions indeed occupy Hf sites. Note that both Fig. 1 and 2 demonstrate peak straightening with temperature,

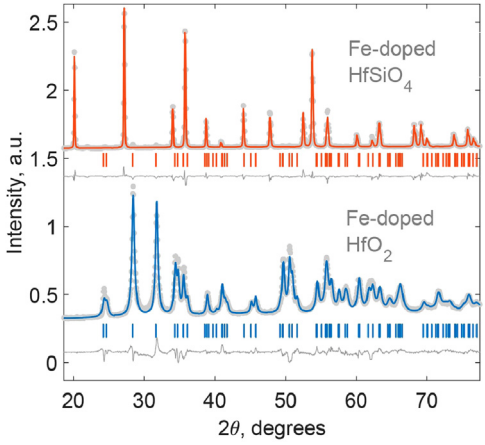

Fig. 2. XRD patterns of Fe doped hafnia straight after calcination (lower) and annealed in a quartz tube at 900 °C (upper).

which likely indicates to the agglomeration of smaller particles into larger grains.

Average size of undoped HfO_2 NPs was estimated with Scherrer formula. Diffraction peaks associated with (11 − 1), (111) and (021) plane sets were used for this analysis and the calculated particle size was 29.53 nm. For iron doped particles we obtained 22.08 nm.

The results of TEM analysis are shown in the Fig. 3. According to transmission microscopy data synthesized hafnia particles have rod-like shape, the average nanorod length being 31.97 nm. Doped particles mostly have spherical or ellipsoidal shape, their size variation range being rather large. Our estimations have given the average size of 14.89 nm. The difference between XRD and TEM results obtained for Fe doped hafnia could have been caused by poorly representative sampling due to the low quality of microscopy image, which did not always allow to distinguish between larger particles and the stacks of smaller specks.

SEM mapping taken after annealing of the doped samples at 900 °C is given in the lhs of Fig. 4. The size distribution was fitted with two-term Gaussian function with the smaller size average of 9.26 μm and the larger one of 24.5 μm.

A more detailed view of annealed Fe-doped hafnia speck can be found in the rhs of Fig. 4. One can distinguish polycrystallites of octahedral (tetragonal di-pyramidal) shape nesting the ∝ 10 μm agglomerate. We have simulated geometrically 5 of these polycrystallites in order to better evaluate their shape parameters. The pyramids were assumed to have square bases with average edge 8.37 μm. The variation of base edge (BE) to pyramid height (H) ratio is shown in the upper part of rhs of Fig. 4, and the average BE/H was found to be 1.4993.

Note that Speer and Cooper have observed similar shape of grown hafnon crystals (Speer and Cooper, 1982). Using the same graphical method for their data we have obtained BE/H = 1.4918. Theoretically, an octahedral crystalite of hafnon with its 8 faces parallel to ± (111), ± (11 − 1), ± (1 − 11), ± (− 111) planes and lattice parameters taken from (Curtis et al., 1954) is expected to have BE/H = 1.5635. Using the parameters obtained for our annealed doped sample with XRD, this ratio was estimated to equal 1.5577. Basing on their geometry and clear XRD results, we hypothesize that the polycrystallites in the Fig. 4 are composed of oriented grains that have hafnon-like structure.

Mass fraction of Si in (S1) sample annealed at 700 °C measured with NAA was 23.7 ± 1 wt% and increased to 32.5 ± 1.2 wt% for hafnia annealed at 900 °C. This remains in agreement with an excess of SiO_2 that appeared at X-ray diffractogram as cristobalite phase. For (S2) sample silicon concentration was determined to be 11.07 ± 0.65 wt% while Fe fraction reached 2.63 ± 0.30 wt% (which corresponds to ~ 17 at%). Assuming no tendency for the creation of an excessive number of oxygen vacancies, one can say that the concentration of Hf in annealed (S2) is ≤ 63.52 wt%. Rounded theoretical mass fractions of Si and Hf in $HfSiO_4$ are 10.38 wt% and 65.97 wt% respectively. Hence, NAA results remain in agreement with our assumption that the dopant preferentially occupies Hf sites, and the migration of Fe ions throughout silicon incorporation is unlikely to occur.

In summary, we emphasize that the tetragonal phase of $HfSiO_4$ for both doped and undoped samples has assembled near 900 °C, a temperature significantly lower than that previously reported for this formation (Curtis et al., 1954; Salt and Hornung, 1967; Choi et al., 2011). We also observed the presence of cristobalite in the samples annealed at 700 °C which is, again, much lower than the known value of 1200 °C required for the formation of this particular phase of quartz (Pluth et al., 1985).

The contribution of high/low cristobalite to the XRD pattern when attempting to synthesize hafnium silicate was reported by many authors (Curtis et al., 1954; Salt and Hornung, 1967; Ramakrishnan et al., 1969; Terry and Tilley, 1991; Kanno, 1993), sometimes even as a major phase (Salt and Hornung, 1967). Whatever silica polymorph taken as precursor (α, β, quartz, amorphous and vitreous silica, etc.), the output blend contained t-SiO_2. There is not much consensus, however, about

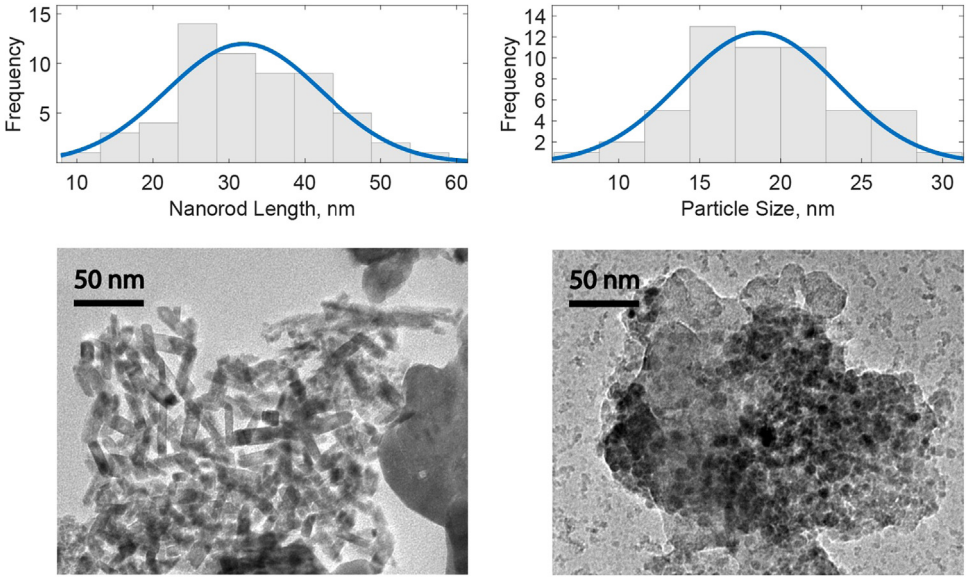

Fig. 3. TEM image and corresponding calculated particle size distributions for undoped (left) and iron doped HfO_2 (right).

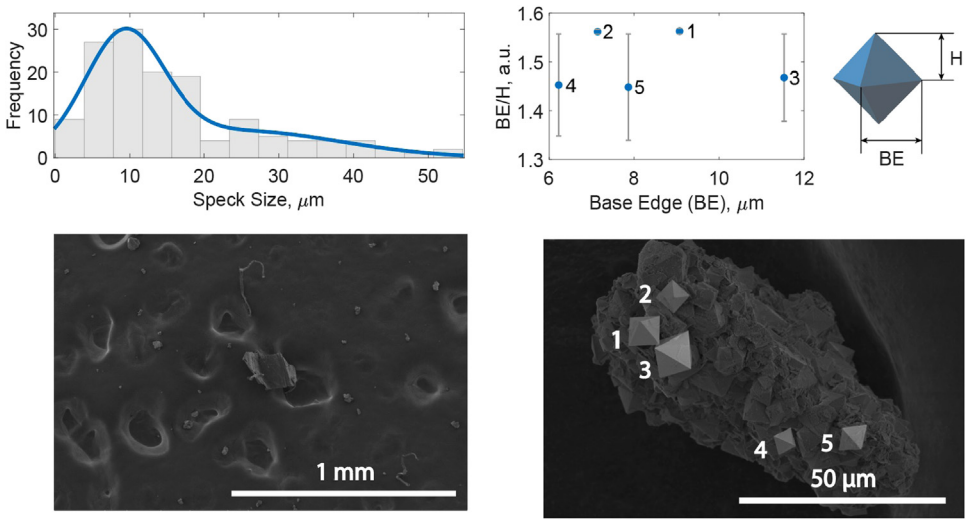

Fig. 4. Fe-doped hafnon grains mapped by SEM with their size distribution (left) and a single speck with highlighted simulated polycrystallites (right). The upper rhs shows the relation between the pyramid height (H) and the length of the base edge (BE), the numbers correspond with those of the crystallites at the SEM image. The error bar shows the difference between the simulated BE/H and that based on the XRD data.

which of the polymorphs favors more the cristobalite formation when exposed to high temperatures in a blend with HfO_2. Also, its concentration was found to depend on annealing temperature and doping. Kanno (1993) demonstrated that doping HfO_2 with Zn and Cu helps the formation of hafnon phase while Mn-doping prevents this formation. They also suggested that the nucleation of cristobalite phase hinders the growth of $HfSiO_4$ and that the longer SiO_2 remains amorphous the easier hafnon would form.

Our study has shown that the contribution of t-SiO_2 decreases with annealing temperature. Fe doping almost eliminates this phase thus providing a more complete crystallization of $HfSiO_4$ at 900 °C. We assume Fe ions at Hf sites to catalyze the formation of hafnon. Herrera et al. (2012) observed similar behavior of $Fe_xZr_{1-x}SiO_4$, the temperature of zircon phase stabilization was decreasing with iron concentration up to $x = 0.07$ (2.1 wt%) where it reached 1100 °C.

An interplay between cristobalite and hafnon phases is evident, and understanding this relation should be crucial to explain the mutual influence of hafnia and silica, the decrease in the formation temperature of $HfSiO_4$ and the role of dopants. Based on our data and cited works, we propose two possible scenarios: (i) in the presence of m-HfO_2 amorphous SiO_2 (a-SiO_2) transforms to t-SiO_2 which, in its turn, interacts with m-HfO_2 until the saturation of the latter to $HfSiO_4$ (no more t-SiO_2 is formed after saturation), i.e. a-SiO_2 + m-HfO_2 $\xrightarrow{T}$ t-SiO_2 + m-HfO_2 $\xrightarrow{T}$ $HfSiO_4$; (ii) there is a competition between two reactions, namely, a -SiO_2 + m-HfO_2 $\xrightarrow{T}$ t-SiO_2 + m-HfO_2 and a-SiO_2 + m-HfO_2 $\xrightarrow{T}$ $HfSiO_4$, the latter prevailing when temperature increases. In the case of (i) we see the decrease in cristobalite peak intensity due to saturation of $HfSiO_4$, whereas if (ii) is true then cristobalite phase is just being formed in smaller amount at higher temperatures (or in the presence of catalysing dopant).

4. Conclusions

An important result of the present work is the development of the method to synthesize hafnon at relatively low temperatures. More precisely, the temperature of phase formation was detected to be about 500 °C lower than that reported previously. We have shown that Fe doping of the initial hafnia NPs provokes the formation of tetragonal $HfSiO_4$ at $T \leq 900$°C. Two possible routes of silica consumption by m-HfO_2 were proposed, and further analysis is needed to give a final explanation of observed phenomenon.

Acknowledgements

This research was partially supported by Fundação de Amparo a Pesquisa do Estado de São Paulo (FAPESP), Brazil (Grant 2014/14001-1). We also appreciate the support of Conselho Nacional de Desenvolvimento Científico e Tecnológico (CNPq), Brazil (Grants 0142271/2014-4, 303808/2014-4 and 304627/2017-8), Coordenação de Aperfeiçoamento de Pessoal de Nível Superior (CAPES), Brazil (Grant 33002010050P7-PNPD), Programa de Capacitação Institucional (PCI), Brazil (Grants 313209/2016-2 and 300066/2017-1) and Comissão Nacional de Energia Nuclear (CNEN), Brazil.

We acknowledge the help and contribution of our colleagues Rafael Henrique Lazzari Garcia (CCN, IPEN-CNEN), Nildemar Aparecido Messias Ferreira (CCTMB, IPEN-CNEN), Thais Bortti Fagundes and Juliana Livi Antoniassi (LCT, Polytechnic College of USP).

References

Amiel, S., 1981. Nondestructive Activation Analysis. Elsiever, Oxford.
Burakov, B., et al., Anderson, E., 2001. Mater. Res. Soc. Symp. Proc. 663 (307), 1–7.
Chen, F.-C., Chu, C.-W., He, J., Yang, Y., 2004. Appl. Phys. Lett. 85 (15), 1251–1257.
Chen, Z., Higgins, D., Yu, A., et al., 2011. Energy Environ. Sci. 4, 3167–3192.
Choi, J., Mao, Y., Chang, J., 2011. Mater. Sci. Eng. 97–136 (R72).
Curtis, C.E., Doney, I.M., Johnson, J.R., 1954. J. Am. Ceram. Soc. 37 (10), 458–465.
Herrera, G., Montoya, N., Alarcón, J., 2012. J. Eur. Ceram. Soc. 32, 227–234.
Ishihara, A., Ohgi, Y., Matsuzawa, K., et al., 2010. Electrochim. Acta 55 (27), 8005–8012.
Kanno, Y., 1993. J. Mater. Sci. Lett. 12 (23), 1807–1809.
Klauk, H., 2010. Chem. Soc. Rev. 39, 2643–2666.
Mecheri, B., Iannaci, A., D'Epifanio, A., et al., 2016. ChemPlusChem 81, 80–85.
Nakano, K., Fukatsu, N., Kanno, Y., 2009. Surf. Coat. Technol. 203, 1997–2002.
Pluth, J., Smith, J., Faber, J., 1985. J. Appl. Phys. 57, 1045–1049.
Ramakrishnan, S.S., Gokhale, K.V.G.K., Subbarao, E.C., 1969. Mater. Res. Bull. 4, 323–328.
Salt, D.J., Hornung, G., 1967. J. Am. Ceram. Soc. 50 (10), 549–550.
de Soete, D., Gijbels, R., Hoste, J., 1972. Neutron Activation Analysis. Willey-Interscience, London.
Speer, J.A., Cooper, B.J., 1982. Am. Mineral. 67, 804–808.
Stassen, A.F., de Boer, R.W.I., Iosad, N.N., Morpurgo, A.F., 2004. Appl. Phys. Lett. 85 (17), 3899–3901.
Terry, K.W., Tilley, T.D., 1991. Chem. Mater. 3 (6), 1001–1003.
Valentin, C., Munoz, M.C., Alarcon, J., 1999. J. Sol-Gel Sci. Technol. 15, 221–230.
Veres, J., Ogler, S., Leeming, W., et al., 2003. Adv. Funct. Mater. 13 (3), 199–204.
Vittadello, M., Negro, E., Lavina, S., et al., 2008. J. Phys. Chem. B 112, 16590–16600.